Title
A damage mechanics assessment of the Larsen B ice shelf prior to collapse: Toward a physically-based calving law

Journal
Geophysical Research Letters, 39(18)

ISSN
0094-8276

Authors
Borstad, CP
Khazendar, A
Larour, E
et al.

Publication Date
2012-09-01

DOI
10.1029/2012gl053317

A damage mechanics assessment of the Larsen B ice shelf prior to collapse: Toward a physically-based calving law

C. P. Borstad,[1] A. Khazendar,[1] E. Larour,[1] M. Morlighem,[2] E. Rignot,[1,2] M. P. Schodlok,[1,3] and H. Seroussi[1]

Received 31 July 2012; revised 22 August 2012; accepted 23 August 2012; published 28 September 2012.

[1] Calving is a primary process of mass ablation for glaciers and ice sheets, though it still eludes a general physical law. Here, we propose a calving framework based on continuum damage mechanics coupled with the equations of viscous deformation of glacier ice. We introduce a scalar damage variable that quantifies the loss of load-bearing surface area due to fractures and that feeds back with ice viscosity to represent fracture-induced softening. The calving law is a standard failure criterion for viscous damaging materials and represents a macroscopic brittle instability quantified by a critical or threshold damage. We constrain this threshold using the Ice Sheet System Model (ISSM) by inverting for damage on the Larsen B ice shelf prior to its 2002 collapse. By analyzing the damage distribution in areas that subsequently calved, we conclude that calving occurs after fractures have reduced the load-bearing capacity of the ice by 60 ± 10%. **Citation:** Borstad, C. P., A. Khazendar, E. Larour, M. Morlighem, E. Rignot, M. P. Schodlok, and H. Seroussi (2012), A damage mechanics assessment of the Larsen B ice shelf prior to collapse: Toward a physically-based calving law, *Geophys. Res. Lett.*, *39*, L18502, doi:10.1029/2012GL053317.

1. Introduction

[2] Iceberg calving from ice shelves and tidewater glaciers represents a significant process of mass ablation from ice sheets. For decades, researchers have sought a general physical law for calving that can be applied in models of ice sheet evolution (for a review, see *Benn et al.* [2007]), yet this important problem in glaciology remains unsolved. This issue was emphasized in the 2007 IPCC Fourth Assessment Report, which indicated that dynamic ice sheet changes, of which calving is an important component, represent the greatest source of uncertainty in projections of sea level rise.

[3] Calving relations or calving laws aim to predict calving events or prescribe the location of the seaward margin based on a set of physical or statistical rules. Since calving is a consequence of fracture, many calving relations are based on a calculation of crevasse depth using fracture mechanics [e.g., *Weertman*, 1973]. Some calving relations are expressions of failure criteria from strength of materials theory [*Benn et al.*, 2007], while others are empirical correlations with the strain rate tensor, ice thickness or water depth [e.g., *Cuffey and Paterson*, 2010]. An alternative foundation for calving models is Continuum Damage Mechanics (CDM), a theory in which a state damage variable accounts for the *effects* of cracks, which are inherently local phenomena, on observables such as deformation or strain rate [e.g., *Murakami and Ohno*, 1981; *Lemaitre*, 1996; *Pralong and Funk*, 2005; *Duddu and Waisman*, 2012]. However, no ice sheet model to date has incorporated CDM to account for interactions between fracture, ice flow and calving.

[4] Here, we couple CDM with the equations of viscous deformation of glacier ice. We invert for damage on the Larsen B ice shelf using remote sensing data obtained prior to the collapse of 2002. Basal melting rates from an ocean circulation model and surface temperature from a regional atmospheric model are used to calculate the ice temperature and parameterize the ice rigidity. The calving threshold is constrained by analyzing damage in areas where tabular calving occurred in the 15 months prior to collapse of the ice shelf. The inversion also provides insight into the mechanical integrity of the ice shelf relevant to its collapse. The scope of the study is limited to proposing the general form of the calving law and determining the calving threshold using observational data; we do not simulate calving events or damage evolution.

[5] We begin with an outline of the damage model and calving criterion, a description of the input data and inversion algorithm, followed by model results and determination of the calving threshold. We conclude by discussing the implications of damage mechanics for assessing ice shelf stability and the relationship between damage and flow enhancement.

2. Damage Model and Calving Criterion

[6] The damage model is derived by replacing the Cauchy stress $\boldsymbol{\sigma}$ by a damage-dependent effective stress $\tilde{\boldsymbol{\sigma}}$ in the governing equations for viscous flow of glacier ice. We assume strain equivalence between the actual material under the applied stress and the equivalent damaged material under the effective stress [*Murakami and Ohno*, 1981; *Pralong and Funk*, 2005; *Duddu and Waisman*, 2012], which leads to the following definition of $\tilde{\boldsymbol{\sigma}}$,

$$\tilde{\boldsymbol{\sigma}} = \frac{\boldsymbol{\sigma}}{(1-D)} \tag{1}$$

where D is the isotropic scalar damage. Damage represents the loss of load-bearing cross sectional area due to fractures [*Murakami and Ohno*, 1981; *Lemaitre*, 1996] and takes values between 0, for fully intact ice, to 1, for ice that is

[1]Jet Propulsion Laboratory, California Institute of Technology, Pasadena, California, USA.
[2]Department of Earth System Science, University of California, Irvine, California, USA.
[3]Joint Institute for Regional Earth System Science and Engineering, University of California, Los Angeles, California, USA.

Corresponding author: C. Borstad, Jet Propulsion Laboratory, California Institute of Technology, 4800 Oak Grove Dr., MS 79-24, Pasadena, CA 91109, USA. (christopher.p.borstad@jpl.nasa.gov)

0094-8276/12/2012GL053317

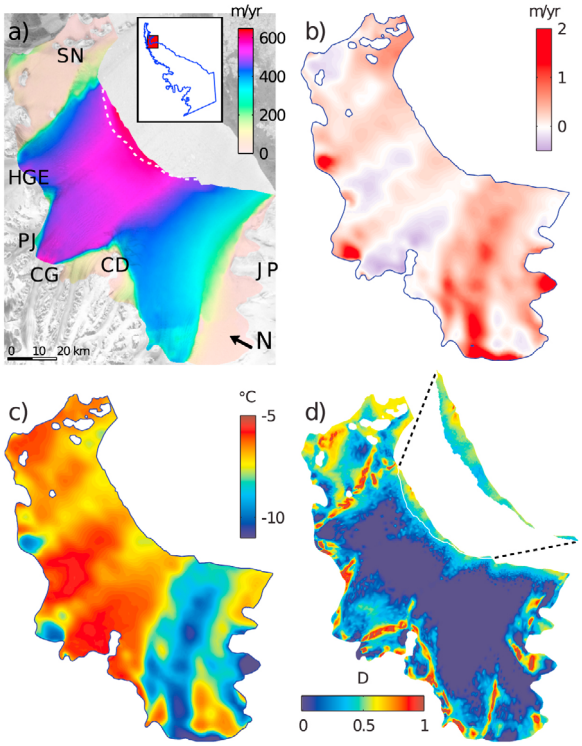

Figure 1. (a) InSAR velocity magnitude observations for Larsen B, fall 2000, overlaid on an earlier radar mosaic of the ice shelf. Inset shows location of ice shelf on Antarctic Peninsula. Dashed white line delimits area that retreated after the velocity observations but prior to the 2002 collapse. Place name acronyms are SN = Seal Nunataks, HGE = Hektoria-Green-Evans Glaciers, PJ = Punchbowl-Jorum Glaciers, CG = Crane Glacier, CD = Cape Disappointment, JP = Jason Peninsula. (b) Calculated basal melting rates (positive for melting, negative for freezing) in meters of ice equivalent per year; (c) depth-integrated ice temperature; (d) inverted damage for a uniform initial state $D_o = 0.4$. Cutout shows area defined in Figure 1a, an area where numerous rifts and crevasses were mapped by *Glasser and Scambos* [2008].

cracked through its full extent. For depth-integrated flow equations, damage represents the influence of both surface and basal crevasses but does not distinguish between the two; only the cumulative effects of fractures on flow are considered. Thus $D = 0.5$ represents a 50% reduction in load bearing capacity due to the integrated influence of fractures within an element.

[7] When the effective stress $\tilde{\boldsymbol{\sigma}}$ is substituted into the momentum balance equations and the common Shallow-Shelf Approximation (SSA) is applied [*MacAyeal*, 1989], the resulting vertically-integrated differential equations take the same form as the SSA equations in all terms except for the ice viscosity ($\bar{\mu}$). Assuming a Glen-type flow law, the viscosity for damaged ice ($\bar{\mu}_D$) becomes [e.g., *Pralong and Funk*, 2005]

$$\bar{\mu}_D = (1-D)\ \ \bar{\mu} = (1-D)\frac{B}{2\,\dot{\varepsilon}_e^{\frac{n-1}{n}}} \tag{2}$$

where B is the ice rigidity, $\dot{\varepsilon}_e$ is the effective strain rate and n is the flow law exponent. Damage affects the boundary condition at the calving front, where seawater pressure opposes ice flow and thus a viscosity term $\bar{\mu}_D$ is present.

[8] In creep damage mechanics, rupture occurs upon reaching a macroscopic brittle instability which can be characterized by a critical or threshold damage D_c [e.g., *Duddu and Waisman*, 2012]. This threshold lies between 0 and 1, where $D_c = 0$ represents fully brittle failure and $D_c = 1$ represents fully ductile failure [*Lemaitre*, 1996]. For polycrystalline ice, D_c has been constrained in the range 0.45–0.56 from creep-rupture experiments [*Pralong and Funk*, 2005; *Duddu and Waisman*, 2012]. For a depth-integrated damage model, as in the present study, D_c represents the onset of a through-thickness failure or calving event. The calving law is thus a common and well-founded failure criterion that arises naturally from formulating the governing equations using damage mechanics.

[9] We constrain D_c by inverting for damage on Larsen B, though the mathematical form of the calving criterion is fully general. We choose Larsen B because its ice front was retreating for over a decade prior to 2002 [*Doake et al.*, 1998; *Rack and Rott*, 2004] and fractures were visible near the ice front 2 years prior to collapse [*Glasser and Scambos*, 2008], therefore velocity data from the same time period should contain a signature of fracture-induced softening. We relate D_c to damage within areas where we map retreat of the ice front between 2000 and 2002 from MODIS images.

[10] To simulate calving events and ice front migration, an additional differential equation describing the initiation, evolution and advection of damage with ice flow is required. Creep damage evolution functions of the Kachanov-Rabotnov type [e.g., *Lemaitre*, 1996] have been successfully applied to polycrystalline ice [*Murakami and Ohno*, 1981; *Pralong and Funk*, 2005; *Duddu and Waisman*, 2012], and though it remains to calibrate such a function for the scale of ice shelf modeling, the theoretical framework is well established. Since a dynamic damage function can have many free parameters, though, calibrating the calving threshold independently using remote sensing data is advantageous from the perspective of eventual model validation and uncertainty analysis.

3. Methods

[11] InSAR surface velocities (Figure 1a) were calculated on a 350 m grid from RADARSAT-1 tracks from fall 2000 (24 day repeat) using speckle tracking techniques. The surface elevation of the ice shelf was taken from the RAMP Antarctic digital elevation model [*Liu et al.*, 1999], with solid ice thickness derived from surface elevation [e.g., *Jenkins and Doake*, 1991]. The surface velocity and elevation data are the same as those used by *Khazendar et al.* [2007] to invert for ice rigidity on Larsen B.

3.1. Basal Melt Rate and Temperature Calculations

[12] Computations of basal melting of the ice shelf were made using the Massachusetts Institute of Technology general circulation model (MITgcm) with a three equation thermodynamic representation of the freezing/melting process in the sub-ice-shelf cavity. The model domain was derived from that of the Estimating the Circulation and Climate of the Ocean, Phase II (ECCO2) project [*Menemenlis et al.*, 2008], but with higher resolution horizontal grid spacing of ~1 km and 60 vertical levels [e.g., *Schodlok et al.*, 2012]. Minor

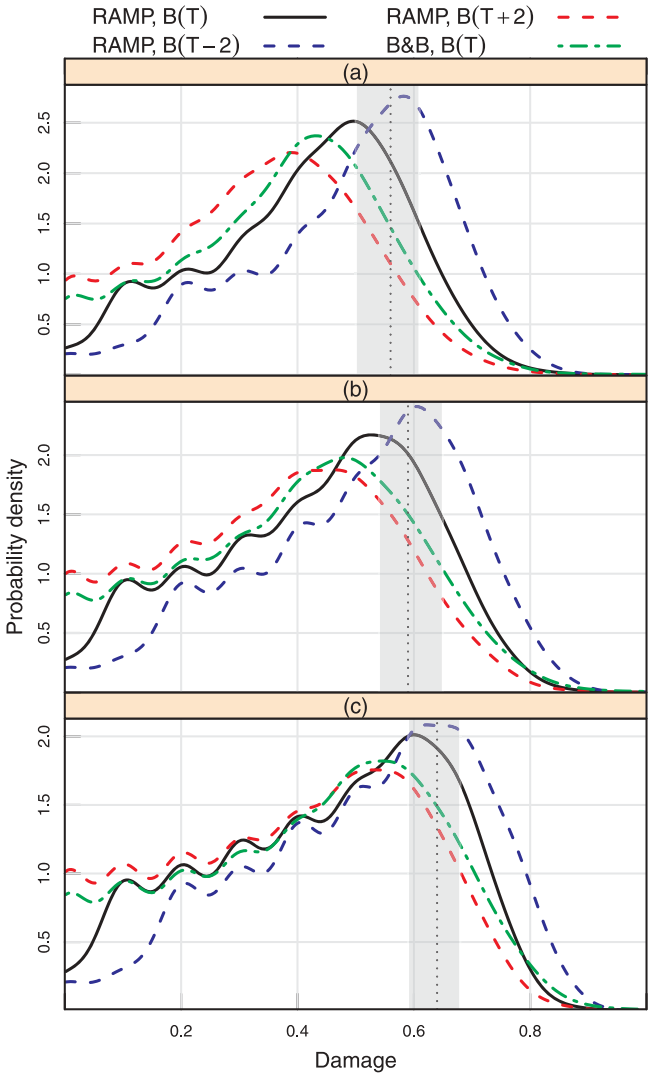

Figure 2. Probability density estimates of damage within the cutout shown in Figure 1d that calved in the 15 months prior to collapse; (a) all nodes (n = 2642) within this area, (b) nodes in the same area but further limited to within 1 km of the ice front (n = 2460), (c) same area, nodes limited to within one ice thickness of the ice front (n = 1150). Results shown using both the RAMP and B&B DEMs [*Liu et al.*, 1999; *Bamber and Bindschadler*, 1997], respectively, as well as for the RAMP DEM with ice rigidity calculated using the outer uncertainty limits of ice temperature. Dotted vertical lines indicate the mean third quartile of the empirical cumulative distribution functions for each panel, with the gray areas representing the spread in individual third quartile values.

modifications were made to the grounding line position to account for differences in resolution between the ocean and ice models. The bathymetry in the sub-ice-shelf cavity was derived from NASA Operation IceBridge data [*Cochran and Bell*, 2012].

[13] A steady state temperature field for the ice shelf was calculated analytically as a function of the melting rates and surface and basal ice temperature, accounting for vertical advection and diffusion of heat into the base of the ice [*Holland and Jenkins*, 1999]. A constant basal temperature of −2°C, the approximate pressure melting temperature, was assumed. The surface temperature was specified using Regional Atmospheric Climate Model (RACMO) mean air temperature data from the period 1980–2004 [*van den Broeke and van Lipzig*, 2004]. The surface temperature was then reduced everywhere by 3°C to tune for the influence of horizontal advection of colder glacier ice into the ice shelf [*Sandhäger et al.*, 2005]. The analytical temperature profile was depth-integrated and used to specify the ice rigidity [*Cuffey and Paterson*, 2010]. The resulting uncertainty in ice temperature is 2°C, which corresponds to a 7–17% uncertainty in ice rigidity.

3.2. Damage Inversion

[14] The inverse method seeks the value of D that minimizes a cost function measuring the misfit between observed and modeled surface velocities. A partial differential equation constrained optimization algorithm is adopted, modified to invert for D rather than total viscosity, analogous to inverting for ice rigidity B [e.g., *Larour et al.*, 2005]. The adjoint state of the model contains a derivative of equation (2) with respect to D, which is the only difference from established algorithms that invert for B [e.g., *Khazendar et al.*, 2007; *Vieli et al.*, 2007]. The algorithm calculates the gradient of the cost function with respect to the unknown and then updates the unknown using a steepest-descent approach. To prioritize convergence near the ice front, the velocity misfit along the ice front is penalized by increasing the cost function by a factor of 100 relative to the rest of the shelf. This weighting has little effect on the damage elsewhere on the ice shelf. The modified inversion routine was implemented in the Ice Sheet System Model (ISSM) [*Larour et al.*, 2012]. The calculations were performed on an unstructured triangular mesh with ~42,000 elements ranging in size from 100 m along the ice front, as well as where the Hessian (second-order partial derivative) of observed surface velocity is highest, to 2000 m. An initial guess D_o is needed for the inversion, and this parameter was varied for sensitivity analysis.

4. Results

[15] The MITgcm melting rates, interpolated onto the finite element mesh, are shown in Figure 1b. Melting rates of about 2 m/yr are produced near the grounding line of the Hektoria-Green-Evans domain and the confluence of Punchbowl-Jorum and Crane Glaciers as well as over extensive regions of the ice shelf to the south of Cape Disappointment. Low rates of freezing are present in the thinner "suture" zones between the major flow units of the ice shelf. The pattern and magnitude of melting agree well with the model results of *Holland et al.* [2009].

[16] The temperature of the ice (Figure 1c) follows a similar pattern as the melt rates, as expected. The coldest ice is in regions with the highest melting rates, a result of the removal by melt of the bottom layer of ice, which is the warmest [*Jenkins and Doake*, 1991]. The ice to the south of Cape Disappointment, which survived the 2002 collapse, is the coldest and thus stiffest ice of the entire ice shelf according to these calculations.

[17] The map of damage from the inversion, given an initial value $D_o = 0.4$ over the whole ice shelf, is shown in Figure 1d. The inversion is sensitive to the initial value of

damage, similar to inversions for ice rigidity [*Khazendar et al.*, 2007]. Inversions were carried out for D_o in the range 0.0 to 0.9 in increments of 0.1. The damage pattern is qualitatively similar and the misfit varies by less than 20% in the range $D_o = 0.2 - 0.6$, but the initial value of $D_o = 0.4$ gives the best fit between modeled and observed velocity. The inner limits of the 2002 collapse, as determined from MODIS images, coincide largely with the weak shear margins of highly damaged ice where $D \approx 1$. These damaged margins are present for inversions at each D_o, and are largely coincident with areas of softer ice inferred by *Khazendar et al.* [2007]. For $D_o = 0.4$, the difference between modeled and observed velocity is within 20 m/yr over the majority of the ice shelf, an agreement of better than 10%.

[18] The determination of the calving threshold takes into account the sensitivity to D_o. Figure 2 shows probability density estimates of damage for nodes within the area that calved between late 2000 and January 2002 (Figure 1). Analyses for this entire area (Figure 2a) as well as limited to nodes within 1 km (Figure 2b) and 1 ice thickness of the ice front (Figure 2c) were performed. Sensitivity of the results to the chosen DEM is studied by running a similar set of inversions using the DEM of *Bamber and Bindschadler* [1997], and sensitivity to temperature is studied by calculating ice rigidity at the $\pm 2^\circ$C uncertainty limits around the calculated depth-integrated ice temperature. For each model setup, 10 inversions were conducted to cover the range in D_o. For each inversion, a probability density estimate of damage for the selected nodes was calculated using a Gaussian kernel. Each curve in Figure 2 represents a weighted average of 10 such individual curves, with the normalized inverse of the velocity misfit as the weighting factor. Thus, inversions which produce better agreement between modeled and observed velocity get more weight in determining the density estimate. The probability densities show evidence of sensitivity to D_o in the localized peaks centered on initial values of D_o below about 0.5. These features are not present for the higher range of D_o, indicating that these levels of damage-induced softening are incompatible with the observed velocity field.

5. Discussion

5.1. Threshold Damage for Calving

[19] The probability density estimates are more sensitive to temperature than to the DEM. The peaks in density are different by as much as 0.2 (Figure 2) over the uncertainty range associated with temperature. These results underline the importance of accurately modeling the thermal regime of an ice shelf, as both temperature and fracture have a strong influence on the ice viscosity.

[20] The probability densities are sensitive to the DEM, underlining the importance of using accurate elevation data. The two DEMs agree to within 2 m on average, with the RAMP DEM slightly lower near the ice front. The small difference in elevations leads to a difference in ice temperature of up to 0.5°C given the dependence on ice thickness in the temperature calculations, which explains part of the difference in density curves.

[21] Despite the spread in curves associated with temperature and the DEM, the third quartiles of the empirical cumulative distribution functions are much more consistent. Moving closer to the ice front within the area that retreated following the velocity observations, i.e., moving from Figures 2a–2c, the mean third quartile value increases and the spread decreases. In Figure 2c, the peaks of the curves are in the closest agreement with the third quartiles, evident by the steeper decline of density to the right of each peak. Assuming that the most likely location for the next calving event is near the ice front, thus giving more weight to the curves in Figures 2b and 2c, we conclude $D_c \approx 0.6 \pm 0.1$.

[22] The common physical interpretation of damage as a loss of load-bearing surface area remains to be verified at the ice shelf scale using observations. It is valid to state that $D_c = 0.6$ corresponds to a 60% reduction in load bearing capacity or, synonymously, in viscosity. This inferred level of softening implicitly includes the influence of factors such as ice fabric, impurities, or the presence of marine ice or meltwater. Furthermore, trains of crevasses or interaction between surface and basal crevasses may combine nonlinearly in determining damage. Therefore, until the importance of these effects can be quantified, it is premature to relate D_c to crevasse depths. Nevertheless, the mathematical form of the calving law established here, which posits failure above a critical level of damage, has general validity for depth-integrated modeling of glaciers and ice shelves.

5.2. Implications of Damage Mechanics for Ice Shelf Stability

[23] In addition to providing a physical representation of calving, damage mechanics has advantages for analyzing the stability of an ice shelf as a whole. For Larsen B, the damage inversion provides a comprehensive view of the mechanical state of the ice shelf prior to its collapse. The influence of fractures is quantified throughout the ice shelf, and the effect of temperature is explicitly separated from that of fracture on the rheology of the ice. Both factors appear to have played an important role in the lead-up to collapse.

[24] The shear margins where $D \approx 1$ (Figure 1d) represent ice weakened through the full thickness of the shelf. These highly damaged regions, which are coincident with observations of rifts and crevasses in satellite imagery from the same time period [*Glasser and Scambos*, 2008], represent lines of weakness in the ice shelf. These structural weaknesses may have played a major role in controlling the flow and stability of the ice shelf by reducing lateral confinement and thus making the ice shelf more susceptible to perturbations at the ice front [*Vieli et al.*, 2007]. North of Cape Disappointment, these damage-softened shear margins coincide with the boundary of the 2002 collapse [*Khazendar et al.*, 2007].

[25] The southern collapse boundary approximately followed the transition between warmer and colder ice extending east of Cape Disappointment (Figure 1c). The area to the south of this boundary that did not collapse is the coldest and stiffest part of the ice shelf. Surface melt features were mostly absent from this region prior to collapse [*Glasser and Scambos*, 2008], in part due to the ice being colder and in part because the air is colder further south. *Khazendar et al.* [2007] inferred softer ice in the suture zone extending from Cape Disappointment, yet no damage was inferred here in this study (Figure 1d). Therefore the calculated temperature field, through the ice rigidity, appears to be sufficient to explain the observed velocity field in this region (neglecting the effects of fabric, marine ice, etc.).

[26] Widespread fractures throughout the ice shelf were observed just one year prior to collapse (P. Skvarca, personal communication, 2005), shortly after our velocity observations. This may explain our finding that much of the interior of the ice shelf shows little or no damage in late 2000 (Figure 1d). Subsequent velocity data may have indicated the softening influence of the observed fractures. Using time-series inversions of damage for existing ice shelves, it should be possible to monitor the spatial and temporal evolution of structural weaknesses arising from fracture-induced softening and temperature changes of the ice.

6. Conclusions

[27] A viscous damage mechanics model was applied to constrain the amount of damage that a floating ice front can sustain. The damage model is a simple modification of the equations for viscous deformation of glacier ice using a scalar damage variable and can be easily implemented in ice sheet models. The formulation explicitly distinguishes between the effects of temperature and fracture on ice rheology. The inferred pattern of damage on the Larsen B ice shelf prior to its 2002 disintegration indicates extensive loss of load bearing capacity along margins that eventually defined the boundary of the collapse. The threshold damage for calving is determined to be $D_c = 0.6 \pm 0.1$. Inverting for damage may prove a valuable tool for monitoring the mechanical integrity of existing ice shelves and will provide initial states for modeling damage evolution—and calving—using established dynamic damage functions.

Appendix A: Damage and Flow Enhancement

[28] The "enhancement factor," sometimes invoked to explain variations in strain rate not accounted for in the flow relation [e.g., *Cuffey and Paterson*, 2010], can be related to damage analytically. The enhancement factor E is a scalar multiplier for the ice softness A, which is equivalent to multiplying the ice rigidity ($B = A^{-1/n}$) by a factor of $E^{-1/n}$, where n is the flow law exponent. Thus E and D are related by

$$E = (1 - D)^{-n}. \tag{A1}$$

If enhancement is linked to fracture-induced softening, equation (A1) provides a physically founded basis on which to specify E. Thus for $n = 3$ and $D = 0.6$, $E \approx 16$.

[29] **Acknowledgments.** CB and HS were supported by appointments to the NASA Postdoctoral Program at the Jet Propulsion Laboratory, administered by Oak Ridge Associated Universities through a contract with NASA. Additional funding provided by the JPL RTD (Research, Technology and Development) program and NASA Cryospheric Science (AK and MS), MAP (Modeling, Analysis and Prediction) and IDS (Interdisciplinary Science) programs.

[30] The Editor thanks an anonymous reviewer for assisting in the evaluation of this paper.

References

Bamber, J. L., and R. A. Bindschadler (1997), An improved elevation dataset for climate and ice-sheet modelling: Validation with satellite imagery, *Ann. Glaciol.*, *25*, 439–444.

Benn, D. I., C. R. Warren, and R. H. Mottram (2007), Calving processes and the dynamics of calving glaciers, *Earth Sci. Rev.*, *82*(3–4), 143–179, doi:10.1016/j.earscirev.2007.02.002.

Cochran, J. R., and R. E. Bell (2012), Inversion of IceBridge gravity data for continental shelf bathymetry beneath the Larsen Ice Shelf, Antarctica, *J. Glaciol.*, *58*(209), 540–552.

Cuffey, K., and W. S. B. Paterson (2010), *The Physics of Glaciers*, 4th ed., Elsevier, Amsterdam.

Doake, C. S. M., H. F. J. Corr, H. Rott, P. Skvarca, and N. W. Young (1998), Breakup and conditions for stability of the northern Larsen Ice Shelf, Antarctica, *Nature*, *391*(6669), 778–780.

Duddu, R., and H. Waisman (2012), A temperature dependent creep damage model for polycrystalline ice, *Mech. Mater.*, *46*, 23–41.

Glasser, N., and T. Scambos (2008), A structural glaciological analysis of the 2002 Larsen B ice-shelf collapse, *J. Glaciol.*, *54*(184), 3–16.

Holland, D., and A. Jenkins (1999), Modeling thermodynamic ice-ocean interactions at the base of an ice shelf, *J. Phys. Oceanogr.*, *29*(8), 1787–1800.

Holland, P. R., H. F. J. Corr, D. G. Vaughan, A. Jenkins, and P. Skvarca (2009), Marine ice in Larsen Ice Shelf, *Geophys. Res. Lett.*, *36*, L11604, doi:10.1029/2009GL038162.

Jenkins, A., and C. S. M. Doake (1991), Ice-ocean interaction on Ronne Ice Shelf, Antarctica, *J. Geophys. Res.*, *96*(C1), 791–813.

Khazendar, A., E. Rignot, and E. Larour (2007), Larsen B Ice Shelf rheology preceding its disintegration inferred by a control method, *Geophys. Res. Lett.*, *34*, L19503, doi:10.1029/2007GL030980.

Larour, E., E. Rignot, I. Joughin, and D. Aubry (2005), Rheology of the Ronne Ice Shelf, Antarctica, inferred from satellite radar interferometry data using an inverse control method, *Geophys. Res. Lett.*, *32*, L05503, doi:10.1029/2004GL021693.

Larour, E., H. Seroussi, M. Morlighem, and E. Rignot (2012), Continental scale, high order, high spatial resolution, ice sheet modeling using the Ice Sheet System Model (ISSM), *J. Geophys. Res.*, *117*, F01022, doi:10.1029/2011JF002140.

Lemaitre, J. (1996), *A Course on Damage Mechanics*, Springer, New York.

Liu, H., K. Jezek, and B. Li (1999), Development of an Antarctic digital elevation model by integrating cartographic and remotely sensed data: A geographic information system approach, *J. Geophys. Res.*, *104*(B10), 23,199–23,214.

MacAyeal, D. (1989), Large-scale ice flow over a viscous basal sediment: Theory and application to Ice Stream B, Antarctica, *J. Geophys. Res.*, *94*(B4), 4071–4087.

Menemenlis, D., C. Campin, P. Heimbach, C. Hill, T. Lee, M. Nguyen, M. Schodlok, and M. Zhang (2008), ECCO 2: High resolution global ocean and sea ice data synthesis, *Mercator Ocean Q. Newsl.*, *31*, 13–21.

Murakami, S., and N. Ohno (1981), A continuum theory of creep and creep damage, in *Creep in Structures*, pp. 422–444, Springer, Berlin.

Pralong, A., and M. Funk (2005), Dynamic damage model of crevasse opening and application to glacier calving, *J. Geophys. Res.*, *110*, B01309, doi:10.1029/2004JB003104.

Rack, W., and H. Rott (2004), Pattern of retreat and disintegration of the Larsen B ice shelf, Antarctic Peninsula, *Ann. Glaciol.*, *39*(1), 505–510.

Sandhäger, H., W. Rack, and D. Jansen (2005), Model investigations of Larsen B Ice Shelf dynamics prior to the breakup, *FRISP Rep.*, *16*, 5–12.

Schodlok, M., D. Menemenlis, E. Rignot, and M. Studinger (2012), Sensitivity of the ice-shelf/ocean system to the sub-ice-shelf cavity shape measured by NASA IceBridge in Pine Island Glacier, West Antarctica, *Ann. Glaciol.*, *53*(60), 156–162, doi:10.3189/2012AoG60A073.

van den Broeke, M. R., and N. P. van Lipzig (2004), Changes in Antarctic temperature, wind and precipitation in response to the Antarctic Oscillation, *Ann. Glaciol.*, *39*(1), 119–126.

Vieli, A., A. J. Payne, A. Shepherd, and Z. Du (2007), Causes of pre-collapse changes of the Larsen B ice shelf: Numerical modelling and assimilation of satellite observations, *Earth Planet. Sci. Lett.*, *259*(3–4), 297–306, doi:10.1016/j.epsl.2007.04.050.

Weertman, J. (1973), Can a water-filled crevasse reach the bottom surface of a glacier?, *IAHS Publ.*, *95*, 139–145.